Inorganic Chemistry

Article

pubs.acs.org/IC

pH-Dependent Coordination of Pb^{2+} to Metallothionein2: Structures and Insight into Lead Detoxification

Yonghui He,[†,⊥,∥] Mengmeng Liu,[†,∥] Narek Darabedian,[§] Yizeng Liang,[†] Deyin Wu,[‡] Juan Xiang,*[,†] and Feimeng Zhou*[,†,§]

[†]College of Chemistry and Chemical Engineering, Central South University, Changsha 410083, People's Republic of China

[‡]State Key Laboratory for Physical Chemistry of Solid Surfaces, Xiamen University, Xiamen 361005, People's Republic of China

[§]Department of Chemistry and Biochemistry, California State University, Los Angeles, California 90032 United States

[⊥]Key Laboratory of Chemistry in Ethnic Medicine Resource, State Ethnic Affairs Commission & Ministry of Education, Yunnan University of Nationalities, Kunming 650031, People's Republic of China

S *Supporting Information*

ABSTRACT: Lead is a toxic heavy metal whose detoxification in organisms is mainly carried out by its coordination with some metalloproteins such as metallothioneins (MTs). Two Pb−MT complexes, named as Pb_7−MT2(I) and Pb_7−MT2(II), form under neutral and weakly acidic conditions, respectively. However, the structures of the two complexes, which are crucial for a better understanding of the detoxification mechanism of Pb−MTs, have not been clearly elucidated. In this Work, coordination of Pb^{2+} with rabbit liver apo−MT2, as well as with the two individual domains (apo−αMT2 and apo−βMT2) at different pH, were studied by combined spectroscopic (UV−visible, circular dichroism, and NMR) and computational methods. The results showed that in Pb_7−MT2(I) the Pb^{2+} coordination is in the trigonal pyramidal $Pb-S_3$ mode, whereas the Pb_7−MT2(II) complex contains mixed trigonal pyramidal $Pb-S_3$, distorted trigonal pyramidal $Pb-S_2O_1$, and distorted quadrilateral pyramidal $Pb-S_3O_1$ modes. The O-donor ligand in Pb_7−MT2(II) was identified as the carboxyl groups of the aspartic acid residues at positions 2 and 56. Our studies also revealed that Pb_7−MT2(II) has a greater acid tolerance and coordination stability than Pb_7−MT2(I), thereby retaining the Pb^{2+} coordination at acidic pH. The higher flexibility of Pb_7−MT2(II) renders it more accessible to lysosomal proteolysis than Pb_7−MT2(I). Similar spectral features were observed in the coordination of Pb^{2+} by human apo-MT2, suggesting a commonality among mammalian MT2s in the Pb^{2+} coordination chemistry.

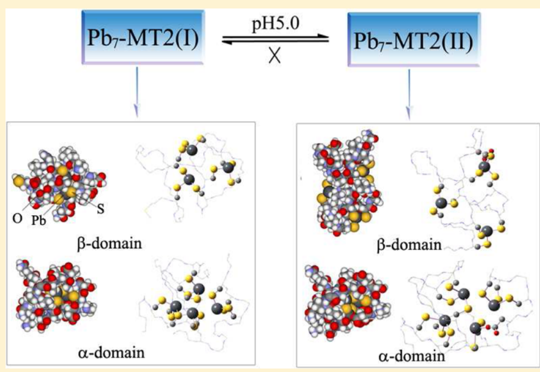

1. INTRODUCTION

Lead poisoning is one of the most serious environmental health hazards, with a particularly acute effect on young children.[1] The U.S. Centers for Disease Control and Prevention estimated that approximately 2.5% of children aged 1−5 years in the U.S. have elevated blood lead levels.[2] The percentage of affected children in other countries is expected to be even higher. Lead poisoning causes learning disabilities, behavioral problems, and, at very high levels, seizures, coma, and even death.[3] Most lead poisoning results from exposure to divalent or "inorganic" lead (Pb^{2+}). The mechanism of Pb^{2+} toxification mainly involves binding of Pb^{2+} to proteins and the subsequent inhibition of the proteins' physiological functions in blood and tissues.[4] The documented proteins targeted by Pb^{2+} include several zinc enzymes or proteins (such as δ-aminolevulinic acid dehydratase (ALAD), acetylcoline esterase, Cys_2His_2 "zinc-finger" proteins, and acid phophatases)[5] and calcium-binding proteins (calmodulin, calbindin, and troponin C).[6] Pb^{2+} can replace zinc and calcium at the oxygen/nitrogen/sulfur-rich active sites of these proteins, thereby inhibiting the protein functions by altering their coordination chemistry and native structures. For example, the function of ALAD, an enzyme involved in the second step of heme biosynthesis, is altered by Pb^{2+} binding at the active site via a trigonal pyramidal geometry. Consequently, the hemoglobin synthesis is blocked, leading to anemia.[7] To reduce the Pb^{2+}-induced toxicity, organisms have developed various defensive mechanisms with species such as metallothioneins (MTs), glutathione, phytochelatins, and lead-binding proteins (PbBPs, which are non-MT acidic proteins that have not been fully characterized).[8] MTs, a class of thiol-rich (up to 30% of its amino acid residues), low-molecular-weight proteins whose abundance is particularly high in the liver and kidneys of mammals,[9] are perhaps the most important species for lead detoxification. They mitigate Pb^{2+} toxicity via formation of stable Pb−MT complexes to protect

Received: September 27, 2013
Published: February 21, 2014

cellular targets such as ALAD.[9] Elucidation of the structures of Pb−MTs is crucial to a better understanding of the chemical stabilities, biological functions, and detoxification mechanism of Pb−MTs. However, due to the absence of single crystals of Pb−MTs, information about the Pb−MTs structures is still scarce.

The coordination and binding stoichiometry between MTs and metals are dependent on the type of metal ions.[10] Usually, divalent metal ions, such as Cd^{2+} and Zn^{2+}, are tetrahedrally coordinated by four cysteine sulfurs and bind to MTs with a stoichiometry of 7:1.[11] Pb^{2+}, however, exhibits a varied coordination behavior. It can be complexed by a combination of S, O, N, and P-donor ligands with a coordination number ranging from 2 to 9.[12] When Pb^{2+} binds to sulfur-rich proteins, three sulfurs in a trigonal pyramidal geometry and the Pb $6s^2$ lone-pair electrons occupying the axial position (hemidirected) constitute the coordination sphere.[13] A number of complexes containing the $Pb-S_3$ coordination have been observed using spectroscopic and mass spectrometry (MS) methods.[14] In the presence of biomolecules possessing several distinct donor ligands (N, O, and S), the Pb^{2+} coordination chemistry is diverse[15] and includes formation of PbS_xO_y and PbS_xN_y. Owing to the presence of O- and S-donor ligands in MTs and the unique electronic configuration of Pb^{2+}, coordination of Pb^{2+} with MT is of higher complexity than that of Zn^{2+} or Cd^{2+}. Previous results from ultraviolet−visible (UV−vis) spectra and microcalorimetry have suggested that different Pb−MT complexes are formed at pH 7.0 and 4.3, respectively.[16] Palacios et al. demonstrated with electrospray ionization mass spectrometry that the metal content in Pb−MT2 complexes is dependent on the solution pH (neutral or 4.5).[17] Using extended X-ray absorption fine structure (EXAFS), Vasak et al. measured the Pb−S distance in Pb−MT complex to be ∼2.65 Å.[18] However, crucial questions such as the difference of Pb^{2+} coordination and the chemical stability and physiological function of the two Pb−MT2 complexes remain to be addressed.

In bioinorganic chemistry, theoretical calculations have been widely used for the prediction of structures and spectra of metalloproteins.[19] The combination of quantum mechanics and molecular mechanics-based hybrid (QM/MM) method allows two or more computational methods to be performed in a single calculation, making it possible to investigate the chemistry of complex systems with high precision.[20] In this context, the ONIOM (our own N-layered integrated molecular orbital + molecular mechanics) scheme is a general approach because it can combine any number of molecular orbital and molecular mechanics methods.[20] The ONIOM method has been successfully utilized in the elucidations of structural and functional properties of many metalloproteins such as Cyt c and azurin.[21] In our Study, optical methods (UV−vis absorption and circular dichroism (CD) spectrometry) and NMR were used in tandem with the two-layer ONIOM method to investigate the effect of pH on the structures of two different Pb−MT2 complexes. The differences in the coordination chemistry of the metal centers and the protein structures at various pH were deciphered. We also investigated the chemical stabilities and structural flexibility of these two complexes in proteolytic processing to gain insight into the lead detoxification process involving MTs.

2. EXPERIMENTAL SECTION

2.1. Reagent. Zn^{2+}-containing MT2, isolated from rabbit liver, was purchased from Hunan Lugu Biotechnology Co. (Changsha, China). Individual metal-free domains (apo-αMT2 and apo-βMT2) of both rabbit liver and human MT2s, and the corresponding mutants (D25N-apo-αMT2 and D2N-apo-βMT2) were synthesized by Shanghai Apeptide Co. (Shanghai, China). All the domains and their mutations were confirmed by mass spectrometry performed by the vendor, and the corresponding purity values (>95%) were determined with HPLC-MS. ^{207}Pb (99.1%) was acquired from Isoflex USA (San Francisco, CA). Lead nitrate, 5,5′-dithio-bis-(2-nitrobenzoate) (DTNB), and cathepsin B were purchased from Sigma-Aldrich (St. Louis, MO). All chemicals were analytical grade. Deionized water with resistivity of 18.2 MΩ cm was collected from a Millipore Simplicity 185 System (Millipore Co., Billerica, MA). All solutions were prepared with deionized water and degassed with nitrogen for at least 30 min.

2.2. Preparation of Apo-MT2. A 3 kDa cutoff Millipore (YM-3) membrane (Millipore, Billerica, MA), equilibrated with 0.01 mol L^{-1} HCl, was used to separate Zn^{2+} from Zn_7−MT2. After spinning at 13 000 rpm for 30 min at room temperature in an Eppendorf 5417R centrifuge (Eppendorf, Hamburg, Germany), the supernatant was used as the apo−MT2 solution. Complete removal of Zn^{2+} from Zn_7−MT2 was confirmed by the disappearance of the characteristic absorption of Zn_7−MT2 at 220 nm.[22] The apo-MT2 concentration was determined by assaying thiol groups with Ellman's reagent, DTNB.[23] Apo−MT2 solution was stored in a nitrogen-saturated flask to avoid thiol oxidation in apo−MT2.

2.3. UV−Vis Absorption and CD Spectroscopies. UV−vis absorption experiments were carried out on a UV-2450 spectrophotometer (Shimadzu, Japan) in quartz cuvettes (1 cm path lengths). CD data were obtained with a Jasco-810 spectrophotometer (JASCO Corporation, Japan).

2.4. Zeta Potential Measurements. Zeta potentials of individual apo-MT2 domains or their mutants were measured at room temperature in a folded capillary cell with a Zetasizer Nano ZS instrument (Malvern Instruments, Southborough, UK). At least four replications were performed for each sample.

2.5. ^{207}Pb NMR Spectroscopy. ^{207}Pb was dissolved with 0.15 M trace metal grade nitric acid (Fisher Scientific) at 250 °C, and the $^{207}Pb(NO_3)_2$ precipitate was collected, dried, and weighed. Appropriate amounts of MT2 (250 μM), KCl (10 mM), and D_2O were mixed under N_2 atmosphere. Both Pb_7−MT2 complexes were prepared by adding $^{207}Pb(NO_3)_2$ to obtain an MT2/Pb^{2+} stoichiometry of 1:7 at corresponding pH (7.0 or 4.0). The resultant solutions were allowed to incubate for 1 h, and the solution pH was brought up to pH 7.0 with KOH. D_2O was added to a final volume of 1 mL, and the solution was transferred to an NMR tube.

All ^{207}Pb NMR spectra were recorded on a Bruker Advance DRX-400 MHz spectrometer at 25 °C using 60° pulses, a 2 s relaxation delay, and a 0.12 s acquisition time (spectral width of 555.6 kHz). A linear prediction was performed to remove the noise, and the real free induction decay (FID) was determined before data processing. After zero-filling, the data (128 000 data points) were processed with an exponential line broadening of 5 Hz using the software TopSpin NMR. The ^{207}Pb NMR chemical shifts are reported downfield from tetramethyllead (δ = 0 ppm; toluene) using 1.0 M $Pb(NO_3)_2$ salt (Fisher) as an external standard (δ = −2990 ppm, D_2O, 25 °C; relative to tetramethyllead).

2.6. Proteolytic Processing of Pb_7−MT2 Complexes. Both Pb_7−MT2(I) and Pb_7−MT2(II) complexes were freshly prepared and diluted in 10 mM KCl solution (pH 7.0) at 37 °C to desired concentrations. Cathepsin B (1.8 ng), with a specific activity of 3000 pmol min^{-1} μg^{-1}, was mixed with 504 pmol of Pb_7−MT2(I) or Pb_7−MT2(II) (the final concentration of Pb^{2+} was 57 μM) in 10 mM KCl solution (pH 5.0). UV absorption spectra were recorded over the entire proteolysis.

2.7. ONIOM Calculations. ONIOM calculations were performed to predict the optimal geometries and electronic absorption spectra of Pb_7−MT2 complexes. All calculations were carried out using the

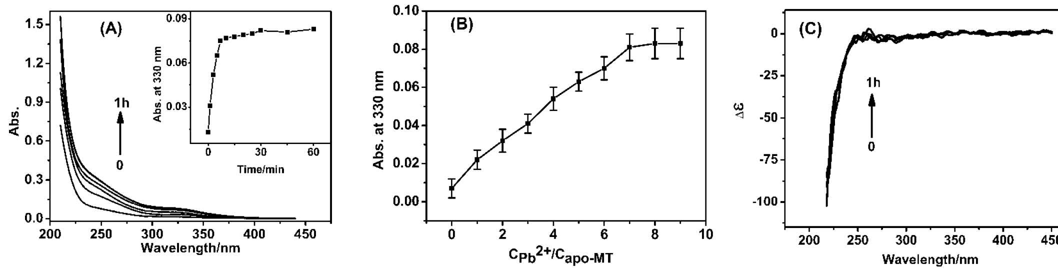

Figure 1. Time-dependent (A) UV−vis absorption and (C) CD spectra in 10 mM KCl solution (pH 7.0) containing 7.20 μM rabbit liver apo-MT2 and 20 mol equiv of Pb^{2+}. (inset) Time-resolved absorbance changes at 330 nm. (B) Dependence of UV absorption peak at 330 nm upon addition of Pb^{2+} to apo-MT2.

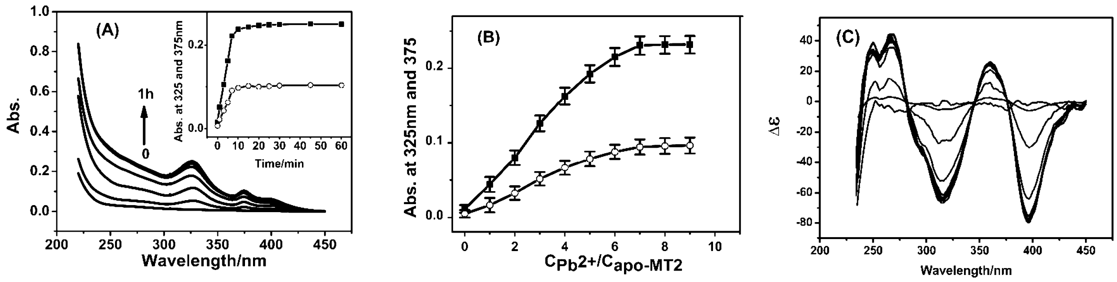

Figure 2. Time-dependent (A) UV−vis absorption and (C) CD spectra in 10 mM KCl solution (pH 4.5) containing apo-MT2 (7.20 μM) and 20 mol equiv of Pb^{2+}. (inset) The time-resolved absorbance changes at 325 and 375 nm, respectively. (B) The dependence of UV absorption peaks at 325 and 375 nm on the addition of Pb^{2+} to apo-MT2.

Gaussian 03 program package.[24] The initial atomic coordinates of Pb_4−αMT2 and Pb_3−βMT2 were taken from the corresponding Pb^{2+}−substituted Cd_4−αMT2 and Cd_3−βMT2, respectively. The structures of Cd_4−αMT2 and Cd_3−βMT2 were retrieved from the RCSB Protein Databank (PDB ID: 1 mrb for the α-domain and 2 mrb for the β-domain), in which the absent hydrogen atoms were added using Gaussview 4.0. The protonation states of titratable residues (e.g., aspartic acid and lysine) of Pb_4−αMT2 and Pb_3−βMT2 at pH 4.0 and 7.0 were determined using pK_a values estimated with PROPKA 2.0.[25]

The electronic structures of Pb_4−αMT2 and Pb_3−βMT2 were modeled with the inclusion of the protein environment, using the two-layer ONIOM (QM/MM) model. The QM region comprises the active sites of Pb_4−αMT2 and Pb_3−βMT2, and the MM region contains the protein environment (cf. detailed compositions in Section 3.2). Two layers were manually specified using Gaussview 4.0.

The geometry optimization was carried out without any symmetry restriction. Spin unrestricted density functional theory (DFT) with the Becke's three-parameter hybrid exchange functional and the Lee−Yang−Parr correlation functional (B3LYP) or pure functional BP86 were used for the QM system, and the Dunning basis set aug-cc-pVTZ-PP was used for Pb and 6-31+G* basis set for other atoms for the QM calculations.[26] For the MM region, the protein molecule was treated using the universal force field (UFF).[27] An electronic embedding scheme was adopted to deal with the electrostatic interactions between the QM and MM regions in the QM/MM calculations.[28]

On the basis of the optimized geometries, vertical excitation energies were computed within the ONIOM scheme by employing the time-dependent density functional theory (TDDFT).[29] TDDFT calculations were carried out with the density functional B3LYP and BP86. The trizeta basis set aug-cc-pVTZ-PP was used for Pb, and 6-31+G** was used for others. The results were transformed via the SWizard program (Version 4.6)[30] into each UV spectrum using Gaussian functions with half-widths of 3000 cm^{-1}.

3. RESULTS AND DISCUSSION

3.1. Spectroscopic Characterization of Pb^{2+} Coordination with Rabbit Liver Apo-MT2. UV−vis absorption and CD spectra were recorded during the titration of rabbit liver apo-MT2 with Pb^{2+} at pH 7.0 (Figure 1). For simplicity, we termed the Pb−MT2 complex formed at neutral pH as Pb−MT2(I). The UV−vis absorption spectrum of Pb−MT2(I) exhibits a characteristic peak centered at 330 nm (Figure 1A). The time-resolved absorbance changes (inset) indicates that the complexation reaction is fast (completed in less than 10 min). During the titration of apo−MT2 with Pb^{2+} at neutral pH, some $Pb(OH)_2$ ($K_{sp} = 1.4 \times 10^{-20}$) precipitate was formed and affected the absorbance value of Pb_7−MT(I) at 330 nm, as evidenced by the small fluctuation even after 30 min. The precipitation can be avoided by lowering the solution pH below 6.0. As shown in the inset of Figure S1 in the Supporting Information, the absorbance value of Pb_7−MT(I) remains stable after the complexation reaction is completed. As indicated by the MT2/Pb^{2+} stoichiometry (Figure 1b), the maximum binding stoichiometry is 1:7, consistent with results reported from the substitution experiment of Zn_7−MT2 with Pb^{2+}.[16b] The absorption wavelength (330 nm) and extinction coefficients ($\varepsilon \approx 3500$ M^{-1} cm^{-1}) of Pb_7−MT2(I) are analogous to values reported for several PbS_3 complexes.[31] The secondary structural variation from apo-MT2 to Pb_7−MT2(I) is shown in Figure 1C. Interestingly, no CD peaks were observed throughout the addition of Pb^{2+}. This is in contrast with the intense CD peaks of Cd_7−MT2 and Zn_7−MT2 between 210 and 290 nm. In Zn_7−MT2, the characteristic CD band centering at 244 nm is attributed to the $Zn(SR)_4$ chromophore. Similarly, the CD bands of Cd_7−MT2 at 242 and 262 nm can be attributed to the excitation coupling between adjacent pairs of the $Cd(SR)_4$ chromophore.[32] Since the $M(SR)_4$ chromophore leads to the appearance of these CD peaks,[32a] the absence of any obvious CD peaks in Figure 1C suggests that Pb_7−MT2(I) adopts a different metal coordination geometry from those of Cd_7−MT2 and Zn_7−MT2, as alluded to in the Introduction. The individual α- and β-domains display UV−vis and CD spectral features (data not shown)

dx.doi.org/10.1021/ic402452s | Inorg. Chem. 2014, 53, 2822−2830

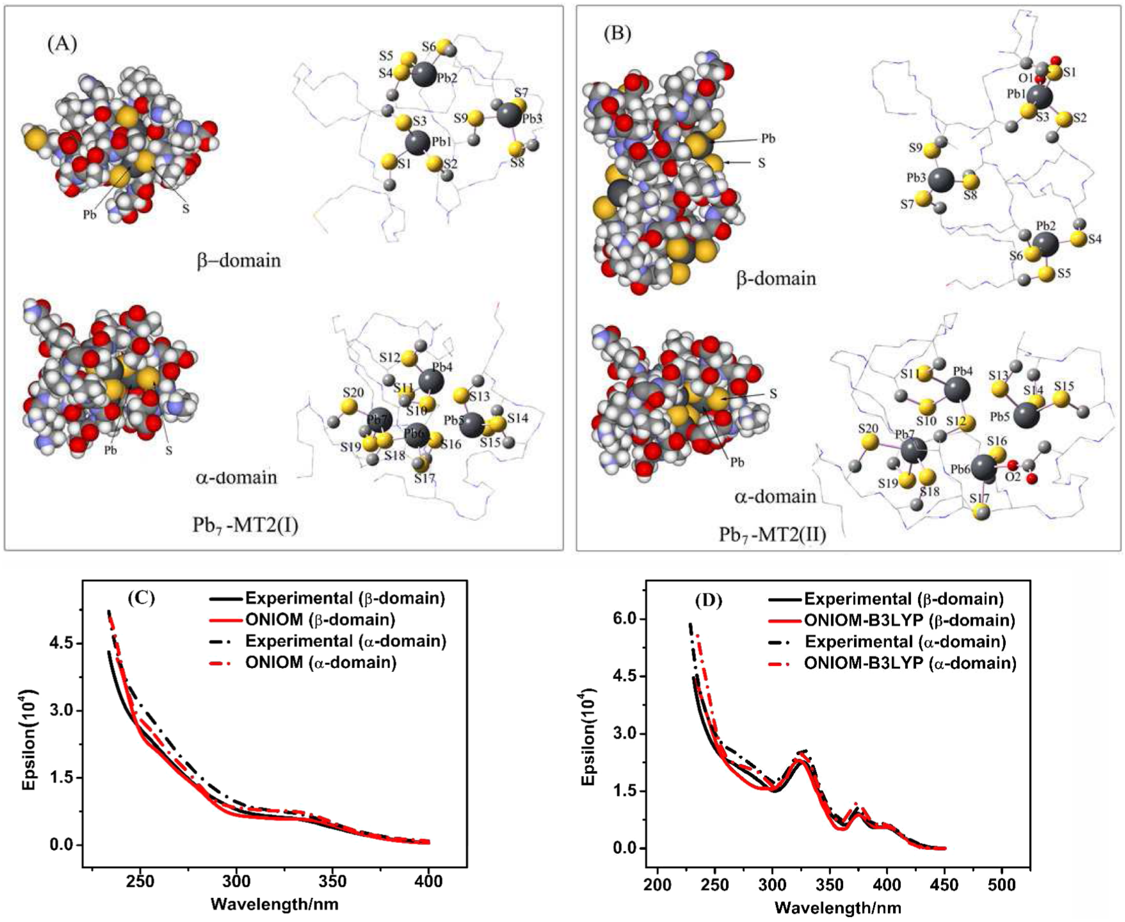

Figure 3. Structures and electronic absorption spectra of the α- and β-domains in (A, C) Pb_7–MT2(I) and (B, D) Pb_7–MT2(II) obtained by experimental and ONIOM methods. In panels A and B, the dark gray spheres are Pb^{2+}, yellow spheres are S, red spheres are O, gray spheres are C, and white spheres are H atoms.

similar to those of apo-MT2 during the titration with Pb^{2+}, indicating that the metal centers in the two different domains have similar coordination spheres. Quantitative analysis confirms that the Pb^{2+}/MT2 stoichiometric ratios are 4:1 and 3:1 in the α- and β-domain, respectively.

We also studied the complex formed at pH 4.5. The Pb_7–MT2(II) complex displays dramatically different UV–vis absorption and CD spectra (Figure 2) from those of Pb_7–MT2(I). In the UV–vis absorption spectra, two intense peaks at 325 and 375 nm appear, with the latter having a shoulder peak at 400 nm. In the CD spectra (Figure 2C), a strong envelope with maxima at 240 (+), 265 (+), 320 (−), 350 (+), 370 (+), and 395 (−) is produced isodichroically (280, 340, and 375 nm). Positions of all CD peaks are invariant with the Pb^{2+}/apo–MT2 ratio (increased stepwise from 1:1 to 7:1), but the peak intensity increases with the ratio. Such behavior is different from that of Cd_7–MT2. The CD spectra of Cd_7–MT2 have two bands at 240 and 260 nm split from the 250 nm band, which corresponds to the conversion of isolated $Cd(SR)_4$ to the $(SR)_3$–Cd–SR–Cd–$(SR)_3$ cluster.[32a] Thus, the unsplittable Pb_7–MT2(II) CD peak is indicative of the absence of excitation coupling between adjacent chromophores. The multiple peaks in the UV–vis absorption and CD spectra suggest that Pb^{2+} in the Pb_7–MT2(II) complex has binding modes that are distinctively different from Cd^{2+} in Cd_7–MT2. Similar to Pb_7–MT2(I), the Pb^{2+}/MT2 stoichiometric ratios in the Pb_7–MT2(II) complex are 4:1 and 3:1 in the α- and β-domains, respectively. The UV–vis absorption peaks of Pb_4–αMT2(II) are slightly shifted, with higher intensity than those of Pb_3–βMT2(II) (Figure 3D). These differences suggest that the metal centers in the two domains have different coordination geometries. To pinpoint the ligands responsible for coordination of Pb^{2+} in the two different domains at neutral and acidic pH, we performed computational studies on the two complexes.

3.2. Structures of Pb_7–MT2 Complexes at Different pH.

The ONIOM method has been successfully used to predict metalloprotein structures.[33] To validate the method for the studies of MT2 structures, structural optimization of Cd_4–αMT2 and Cd_3–βMT2 models were first performed. Compared to the NMR results,[34] the computed structures of the metal clusters display little deviation (e.g., the bond lengths have a root-mean-square deviation of only 0.04–0.05 Å when compared to the experimental data) (Figure S2 and Table S1 in Supporting Information). Therefore, we conclude that the ONIOM method is viable for the studies of the two Pb_7-MT2 complexes.

The theoretical calculations were performed separately on the α- and β-domains on the basis that the two domains are structurally independent. The initial atomic coordinates of each domain in Pb_7–MT2 were respectively adopted from the Pb^{2+}-substituted Cd_4–αMT2 and Cd_3–βMT2 because a well-established model of apo-MT2 is not available. The protonation states of titratable residues (e.g., Asp and Lys) at different pH

dx.doi.org/10.1021/ic402452s | Inorg. Chem. 2014, 53, 2822–2830

Table 1. The Pb−S Bond Lengths in Pb_7−MT2(I) Calculated with B3LYP

	bond length (Å)		bond length (Å)		bond length (Å)
Pb1−S1	2.633	Pb1−S2	2.701	Pb1−S3	2.613
Pb2−S4	2.706	Pb2−S5	2.719	Pb2−S6	2.651
Pb3−S7	2.669	Pb3−S8	2.710	Pb3−S9	2.702
Pb4−S10	2.653	Pb4−S11	2.702	Pb4−S12	2.713
Pb5−S13	2.712	Pb5−S14	2.682	Pb5−S15	2.652
Pb6−S16	2.689	Pb6−S17	2.693	Pb6−S18	2.729
Pb7−S18	2.737	Pb7−S19	2.631	Pb7−S20	2.678

Table 2. The Pb−S and Pb−O Bond Lengths in Pb_7−MT2(II) Calculated with B3LYP

	bond length (Å)		bond length (Å)		bond length (Å)		bond length (Å)
Pb1−S1	2.939	Pb1−S2	2.848	Pb1−S3	2.803	Pb1−O1	2.480
Pb2−S4	2.741	Pb2−S5	2.676	Pb2−S6	2.738		
Pb3−S7	2.712	Pb3−S8	2.721	Pb3−S9	2.743		
Pb4−S10	2.753	Pb4−S11	2.712	Pb4−S12	2.720		
Pb5−S13	2.720	Pb5−S14	2.734	Pb5−S15	2.745		
Pb6−S16	2.852	Pb6−S17	2.838	Pb6−O2	2.247		
Pb7−S18	2.715	Pb7−S19	2.758	Pb7−S20	2.738		

were determined from the pK_a values estimated with PROPKA 2.0.

In the two-layer ONIOM model of Pb_7−MT2(I), the QM region consists of four Pb atoms, and the side chains consist of eleven cysteine residues in the α-domain. As for the β-domain, the three Pb atoms and the side chains of nine cysteine residues constitute the QM region. The remaining atoms are in the MM region. Figure 3A displays the optimized molecular geometries of the α- and β-domains in Pb_7−MT2(I), which are quite different from the well-characterized Cd_7−MT2 and Zn_7−MT2 structures. In Cd_7−MT2 and Zn_7−MT2, each metal adopts the tetrahedral coordination with terminal and bridging thiolates to form a metal−ligand six-membered ring in the β-domain and two fused six-membered rings in the α-domain.(cf. Figure S2 in Supporting Information) However, all seven Pb^{2+} ions in Pb_7−MT2(I) are trigonally coordinated by three cysteine sulfurs ($Pb-S_3$) without any metal−ligand ring in the α- or β-domain. These significant differences can be attributed to the Pb $6s^2$ lone-pair electrons, which disrupt the tetrahedral coordination by occupying the axial position with a significant stereochemical activity. This point is in line with the report by Godwin and co-workers, who stated that $Pb-S_4$ is not a preferred coordination and that trigonal pyramidal geometry in all-sulfur coordination is predominant.[13] Moreover, due to the $Pb-S_3$ coordination, only one bridging cysteine (Pb6−S18−Pb7 in the α-domain) remains, preventing a Pb−S metal−ligand ring from forming. According to the corresponding structural parameters (Table 1), the average length of the Pb−S bonds is 2.68 Å, close to the reported EXAFS value (2.65 Å).[18] The electronic absorption spectra (red line curves), simulated by TDDFT using the B3LYP functional, are overlaid with the experimental results (black line curves) in Figure 3C. The agreement between the simulation and experimental data in the oscillator strengths indicates that the optimized molecular geometries of $Pb_4-\alpha$MT2(I) and $Pb_3-\beta$MT2(I) are reasonable. Detailed analysis of vertical excitation energies, oscillator strengths, and molecular orbital contributions (Table S3 in Supporting Information) indicated that four transitions contribute to the absorption peak at 330 nm. These transitions are HOMO→LUMO, HOMO-1→LUMO, HOMO-2→LUMO, and HOMO-1→LUMO+1. From the frontier molecular orbitals (Figure S3 in Supporting Information), LUMO and LUMO+1 (the final state of the transitions) are mainly located at the Pb−S bonds, while HOMO and HOMO-1 (the initial states of the transitions) are largely localized at the sulfur atoms. Therefore, the electronic absorption band at 330 nm can be attributed to the $S\rightarrow Pb^{2+}$ ligand-to-metal charge transfer (LMCT).

In the two-layer ONIOM model of Pb_7−MT2(II), we initially assigned the QM region of each domain to be the same as that of Pb_7−MT2(I). However, the optimized molecular geometries revealed two unexpected short Pb/O distances (5.52 Å for Pb1 with the carbonyl oxygen of Asp2 in the β-domain and 4.31 Å for Pb6 with the carbonyl oxygen of Asp56 in the α-domain). These short distances should result from the electrostatic interaction between the protein surface (the MM region) and the negatively charged Pb−S cluster (the QM region).[35] Under acidic pH conditions, the protein surface is neutral or positively charged, causing the MM and QM regions to move closer, thereby shortening the distance between the Pb−S cluster and the Asp residue. Moreover, based on the pK_a values of Asp (∼4.00), both Asp residues are neutral in weakly acidic solution, which are more favorable than the negatively charged (deprontonated) form to the positioning of the negatively charged Pb−S clusters in close proximity. These Pb/O distances are close to the sum of the van der Waals radius of Pb and O (3.54 Å),[36] indicating the Pb···O interaction must be taken into account. We therefore modified the initial QM region in each domain by including the respective Asp residue.

As shown in Figure 3B, the optimized molecular geometry of Pb_7−MT2(II) shows an entirely different coordination sphere from that of Pb_7−MT2(I). The overall coordination sphere includes the trigonal pyramidal $Pb-S_3$ mode, the distorted trigonal pyramidal $Pb-S_2O_1$ mode in the α-domain, and the distorted quadrilateral pyramidal $Pb-S_3O_1$ in the β-domain. The Pb $6s^2$ lone pair electrons occupy the axial position with a significant stereochemical activity, resulting in hemidirectionality in the Pb−ligand coordination. All 20 cysteine sulfurs in Pb_7−MT2(II) coordinate Pb^{2+} in the terminal form. Moreover, due to protonation of the peptide side chain, several cysteine sulfurs (especially in the β-domain) are closer to the protein exterior and increase the effective radius of the metal center and the Pb−S bond length (cf. Table 2). The same tendency has

dx.doi.org/10.1021/ic402452s | Inorg. Chem. 2014, 53, 2822−2830

been shown in the demetalation process of MT2.[37] The loosened structure of the metal center renders a higher flexibility to Pb_7−MT2(II). The simulated oscillator strengths are in good agreement with the experimental data (Figure 3D), indicating that the optimized molecular geometries of Pb_4−αMT2(II) and Pb_3−βMT2(II) are reasonable. The small deviation between the electronic absorption spectra of the two domains (cf. Figure 3D) can be attributed to the different coordination geometries. Detailed vertical excitation energies and molecular orbital contributions (Table S5 and Figure S4 in Supporting Information) indicate that all three bands are primarily associated with the S→Pb^{2+} LMCT.

Note that all of the above calculations are based on B3LYP, a hybrid functional to fit data primarily for main-group elements.[38] Because of the large exact exchange component (20%), B3LYP is known to favor loose electron densities and low transition energies. To confirm the reliability of B3LYP, the pure functional BP86, a generalized-gradient approximation (GGA) class with zero exact exchange,[38a,39] is used as a control study on the geometry optimization and calculations of the excited states for both Pb_7−MT2 complexes. The simulated structures of both Pb_7−MT2 complexes from BP86 pure functional (Table S6−9 in Supporting Information) are similar to those from B3LYP hybrid functional. However, the spectra from BP86 pure functional display a significant deviation from the experimental data (Figure S5 in Supporting Information), indicating that the B3LYP hybrid functional is a better choice. The B3LYP hybrid functional produces better spectral accuracy, which can be attributed to its increased amount of Hartree−Fock (HF) exchange.

Another point worth mentioning is the "local minima" in the QM optimization. In the QM/MM calculation of biomolecules, the vast size of the available configuration space may cause the QM optimization to stop at local minima. One way to circumvent this problem is to use a reliable structure (e.g., a structure deduced from NMR or X-ray crystallography) at the beginning of the QM optimization.[19] For instance, Subramanian et al. have used the X-ray structure of azurin as the initial structure in the QM/MM calculation of metal-substituted azurins and obtained noticeable structural changes on the active sites when Cu^{2+} in azurin was substituted by metal ions such as Co^{2+}, Ni^{2+}, or Zn^{2+}.[33a] We adopted this approach by using the Pb^{2+}-substituted Cd_4−αMT2 and Cd_3−βMT2 structures deduced from the NMR experiments[34] as the initial structures. The theoretical spectra agree well with the experimental results, suggesting a high level of reliability of the calculation and in the predicted structures.

3.3. NMR and Mutational Studies of the Pb_7−MT2 Complexes. To provide more experimental evidence to our computational results about the two different Pb_7−MT2 complexes, we conducted ^{207}Pb NMR in solutions of the two complexes (Figure 4). Pb_7−MT2(I) displays one ^{207}Pb peak at 5679 ppm, while Pb_7−MT2(II) exhibit two peaks at 5820 and 4348 ppm. Thus it is clear that the Pb^{2+} coordination in these two complexes are different. Furthermore, the ^{207}Pb signal of Pb_7−MT2(I) at 5679 ppm is well within the chemical shift region (from 5600 to 5800 ppm) where PbS_3 species with the trigonal pyramidal coordination are observed.[14c,31a] Thus we conclude that PbS_3 is the binding mode in Pb_7−MT2(II). For Pb_7−MT2(II), the peak at 5820 ppm is also assigned to the PbS_3 coordination, given its close vicinity to the 5600−5800 ppm region. Compared to the Pb_7−MT2(I) peak, the shift by 141 ppm can be attributed to the changes of the

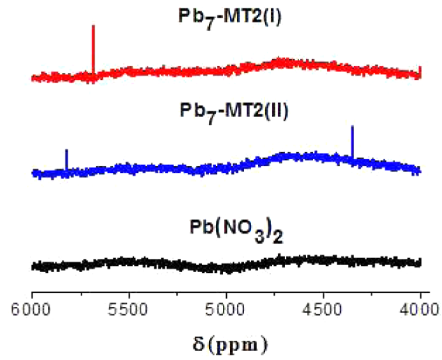

Figure 4. ^{207}Pb NMR spectra of (red) Pb_7−MT2(I), (blue) Pb_7−MT2(II), and (black) $Pb(NO_3)_2$ at pH 7.0.

aforementioned Pb−S bond length and the S−Pb−S bond angle in the PbS_3 coordination. The lower intensity is indicative of the decreased number of PbS_3 clusters in Pb_7−MT2(II). The conversion of metal centers in the PbS_3 coordination to a different binding mode contributes to the appearance of the peak at 4348 ppm. It is well-known that the NMR signal of ^{207}Pb bound to O-containing ligands is shifted upfield with respect to that bound to S-containing ligands.[40] We therefore assign the peak at 4383 ppm to the PbS_3O_1 coordination.

The carbonyl group of Asp is the only O-donor ligand in MT2. To further verify the formation of the Pb−O bond in Pb_7−MT2(II), a titration was performed by adding Pb^{2+} into a peptide solution whose Asp residue had been mutated with Asn (i.e., D25N-apo-αMT2 and D2N-apo-βMT2). Zeta potential and CD measurements did not show discernible changes in the surface charge and structure of both mutants (Figure S6 and S7 in Supporting Information), confirming the viability of these mutants for coordination studies. At neutral pH, both UV−vis absorption and CD spectra of the two mutants show features similar to those in the same spectra of Pb_4−αMT2(I) and Pb_3−βMT2(I), verifying that Asp does not participate in the Pb^{2+} coordination in Pb_7−MT2(I). At acidic pH (pH < 5), the UV−vis absorption spectra of both mutants display only a single peak at 330 nm, and the CD spectra did not reveal any changes. While these features are rather different from the corresponding spectra of Pb_4−αMT2(II) and Pb_3−βMT2(II), they are analogous to those of Pb_4−αMT2(I) and Pb_3−βMT2-(I). We therefore conclude that Asp is involved in the coordination of Pb^{2+} in Pb_7−MT2(II). The unique UV−vis absorption spectra of Pb_7−MT2(II), with multiple peaks and the presence of a new ^{207}Pb NMR peak at 4348 ppm, are well-correlated with the mutational study.

Another piece of evidence for the formation of Pb−O bond is the transition from a single peak to three peaks in the time-dependent spectra of a mixture of Pb^{2+}/apo-MT2 at pH 4.5−5.0 as well as the appearance of multiple peaks in the CD spectra (cf. Figure 5). These changes are indicative of the transition from the Pb−S_3 coordination mode to those containing Pb−S_3, Pb−S_2O_1, and Pb−S_3O_1. Preferential formation of Pb−S_3 has been attributed to the high enthalpy of the Pb−S bond formation,[41] which makes the structure thermodynamically favored. However, because of the negative impact of acidity on the formation of the Pb−S bond (cf. the proton-releasing process shown in reaction 1) and the rearrangement of the peptide chain, the Pb−S_3 formation rate decreases inversely with pH. Therefore, under more acidic conditions (pH < 4.5), the time-dependent peak transition

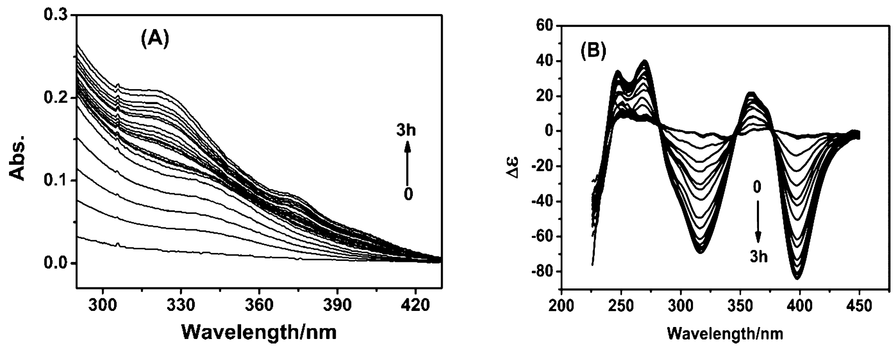

Figure 5. Time dependence of (A) UV−vis absorbance and (B) CD spectra in a KCl solution after the addition of 7 mol equiv of Pb^{2+} to an apo-MT (7.20 μM) solution at pH 5.0. Reaction times from bottom to top: 0, 1, 3, 5, 7, 10, 15, 20, 25, 30, 45, 60, 75, 90, 105, 120, 135, 150, 175, and 180 min.

disappears, and the spectra show features typical of Pb_7−MT2(II).

$$Pb^{2+} + 3R{-}SH \rightarrow 3Pb - (S{-}R)_3 + 3H^+ \quad (1)$$

3.4. Stabilities of Pb_7−MT2 Complexes at Different pH. To study the acid tolerance of both Pb_7−MT2 complexes, a series of spectrophotometric titrations at different pH was performed. The corresponding complex was confirmed by the appearance of characteristic UV−vis absorption peaks of Pb_7−MT2(I) or Pb_7−MT2(II). The results show that Pb_7−MT2(I) is formed above pH 5.0, whereas Pb_7−MT2(II) is produced at more acidic pH. Pb_7−MT2(I) can be transformed to Pb_7−MT2(II) by adjusting the solution pH to 5.0 or lower. However, once Pb_7−MT2(II) is formed, it remains stable at neutral pH. Our demetalation experiments (Figure S8 in Supporting Information) indicate that pH 2.5 is sufficiently low for the complete removal of Pb^{2+} from Pb_7−MT2(I), but stripping Pb^{2+} completely of Pb_7−MT2(II) requires a pH as low as 2.0. These results (summarized schematically in Figure 6) indicate that Pb_7−MT2(II) has a higher tolerance toward an acidic environment than Pb_7−MT2(I) has. Moreover, Pb_7−MT2(II) remains stable even in the presence of apo-MT at neutral pH (data not shown). We believe that the greater acid tolerance and higher structural stability of Pb_7−MT2(II) results from the Pb−O bond. Such a finding has a significant implication to the lead detoxification process in physiological milieu.

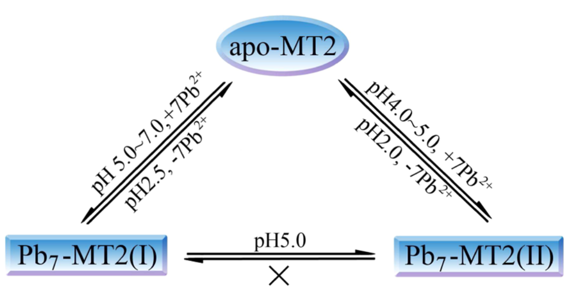

Figure 6. Transformation among apo−MT2, Pb_7−MT2(I), and Pb_7−MT2(II).

The Pb^{2+}-inflicted toxicity stems from its tight binding to a variety of sulfur-rich proteins, such as GATA proteins and the steroid receptor DNA-binding domains. Pb^{2+} replaces Zn^{2+} in these proteins and diminishes their native protein function.[42] MT2 reduces the Pb^{2+}-inflicted toxicity by seizing free Pb^{2+} or sequestering Pb^{2+} from these proteins to recover the native protein function. Higher acid tolerance and greater structural stability render MT2 a greater power in effectively scavenging Pb^{2+} in different environments. As shown in reaction 1, Pb^{2+} sequestration by apo−MT2 accompanies the release of H^+, which in turn increases the acidity in a highly localized region (e.g., in cytosol). Moreover, it has been reported that elevated Pb^{2+} concentrations induce the stress level of various organisms, and acidity is also correlated with the stress level.[43] We posit that Pb_7−MT2(II) is more effective than Pb_7−MT2(I) in lead detoxification, given its greater structural stability and acid tolerance.

3.5. Proteolytic Processing of the Pb_7-MT2 Complexes. Elucidation of the metabolism of the Pb-MT complexes is vital for understanding the lead detoxification by MTs. Some reports have suggested that exogenous MT is processed mainly by the lysosomal protease, and the rate of MT degradation is dependent on the types of metals bound by MTs.[44] Four different cathepsins have been identified in lysosomes, and the cysteine protease (cathepsin B, L, and H) is the principal protease for MT degradation.[45] We used cathepsin B for the proteolytic processing of both Pb_7−MT2 complexes. Variations in the concentrations of the two Pb_7−MT2 complexes in the presence of cathepsin B were measured by UV−vis absorption spectrometry. In Figure 7, the Pb_7−MT2 concentrations were normalized with respect to their initial concentrations. Within 120 min, Pb_7−MT2(II) is degraded 2 times more than Pb_7−MT2(I). Such a higher degradation rate can be attributed to the more flexible structure of the Pb_7−

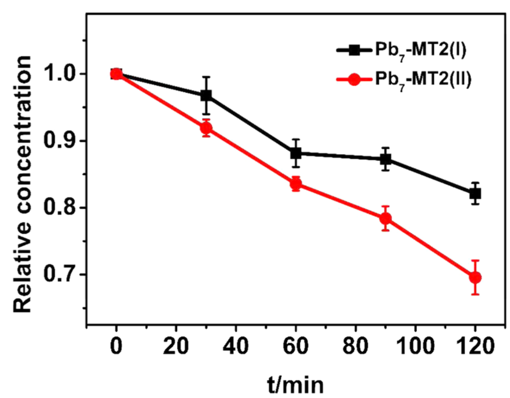

Figure 7. Time-dependent proteolytic processing of (black) Pb_7−MT2(I) and (red) Pb_7−MT2(II) by cathepsin B.

dx.doi.org/10.1021/ic402452s | Inorg. Chem. 2014, 53, 2822−2830

MT2(II) complex. Cathepsin B is an endopeptidase that cleaves internal peptide bonds and favors a large hydrophobic side chain in the substrate protein.[44] Side chains on the amino acids dock into the cathepsin's subsites, whose interaction with the protein substrate is dependent on the flexibility of substrate protein.[46] In MTs, the existence of bridging cysteine sulfurs compacts the metal center, which dominates the protein folding.[47] In Pb_7−MT2(II), due to the lack of bridging cysteine sulfurs, the metal center is loosened, which improves the flexibility of the protein. Moreover, when the Pb−O bond is formed, the geometries of Pb−S_2O_1 and Pb−S_3O_1 become distorted. Consequently, Pb^{2+} ions are positioned farther from the cysteine sulfurs, and the Pb−S bonds are weakened. Both processes facilitate the conformational adjustment of Pb_7−MT2(II). The significantly improved flexibility of Pb_7−MT2(II) facilitates the protein in the "induced-fit" model with cathepsin B.[48] As a result, the proteolytic processing of Pb_7−MT2(II) is greatly accelerated. In living organisms, the acidity in lysosome is about 5, which is sufficiently low to cause the structural conversion from Pb_7−MT2(I) to Pb_7−MT2(II) and to accelerate the degradation of Pb−MT2 complexes. Such processes are beneficial to the effective detoxification and metabolism of Pb^{2+}.

The coordination of Pb^{2+} with individual human apo−MT2 or apo−MT3 domains at different pH was also studied by UV−vis absorption and CD spectrometry. The pH-dependent spectral features were only observed for the apo−MT2 domain (Figure S9 in Supporting Information). Mutational studies revealed that the Asp residue is also essential for the pH-dependent structural variation. In line with the data observed for the rabbit liver MT2, the structure-dependent chemical and biological activities of Pb_7−hMT2(II) formed between human MT2 and Pb^{2+} have higher acid tolerance, more coordination stability, and faster proteolytic processing than Pb_7−hMT2(I) (Figure S10 in Supporting Information). Our results suggest that there exists a commonality in the Pb^{2+} coordination chemistry among mammalian MT2s.

4. CONCLUSION

In this Work, the pH-dependent coordination chemistry between Pb^{2+} and MT2 was systematically studied. The combination of spectroscopic studies and ONIOM calculations provided a detailed description of the two different Pb_7−MT structures. The results and structures were further verified by ^{207}Pb NMR and mutational experiments. The similar structural, chemical, and biological properties between rabbit liver Pb_7−MT2(II) and human Pb_7−MT2(II) suggest a commonality in the Pb^{2+} coordination chemistry among mammalian MT2s. The higher acid tolerance, greater coordination stability, and faster degradation rate of Pb_7−MT2(II) have significant implications for the Pb^{2+} detoxification process. Specifically, MT2 reduces the Pb^{2+}-inflicted toxicity by seizing free Pb^{2+} in the cellular milieu or by sequestering Pb^{2+} from Pb^{2+}-inflicted proteins. The unique properties of Pb_7−MT2(II) render MT2 a greater power to effectively scavenge Pb^{2+} in different environments (e.g., in a localized acidic cytosol region). Moreover, the greater flexibility of Pb_7−MT2(II), resulting from the absence of bridging cysteine sulfurs, helps to accelerate its processing by lysosomal protease. The structural conversion from Pb_7−MT2(I) to Pb_7−MT2(II) is likely to occur in the acidic environment of lysosome, facilitating the effective detoxification and metabolism of Pb^{2+}.

■ ASSOCIATED CONTENT

Ⓢ Supporting Information

Calculated structural parameters and electronic transition data, zeta potentials, and additional circular dichroism and UV−vis absorption spectra. This material is available free of charge via the Internet at http://pubs.acs.org.

■ AUTHOR INFORMATION

Corresponding Authors

*E-mail: xiangj@csu.edu.cn (J.X.).

*E-mail: fzhou@calstatela.edu (F.Z.).

Author Contributions

[‖]Y.H. and M.L. contributed equally.

The manuscript was written with contributions from all authors. All authors have given approval to the final version of the manuscript.

Funding

This Work was supported by the National Natural Science Foundation of China (21273288 and 20773165 to J.X.), the National Key Basic Research Program of China (2014CB744502), the National Science Foundation (NSF 1112105 to F.Z.), a grant from the National Institutes of Health (SC1NS070155−01 to F.Z.), and the Specialized Research Fund for the Doctor Program of Higher Education (20120162110018 to J.X.).

Notes

The authors declare no competing financial interest.

■ ACKNOWLEDGMENTS

We are grateful for the technical support from the High Performance Computing Center of Central South University. We thank Dr. Ali Jabalameli for his help on the NMR experiment.

■ REFERENCES

(1) Loghman-Adham, M. *Environ. Health Perspect.* **1997**, *105*, 928−938.

(2) Krezel, A.; Maret, W. *J. Am. Chem. Soc.* **2007**, *129*, 10911−10921.

(3) (a) Greenwood, N. N.; Earnshaw, A. *Chemistry of the Elements;* Butterworth Einemann: Boston, MA, 1997. (b) Harrison, R. M.; Laxen, D. P. H. *Lead Pollution;* Chapman and Hall: London, U.K., 1981.

(4) Stillman, M. J.; Shaw III, C. F. *Metallothioneins;* VCH: New York, 1992.

(5) (a) Simons, T. J. *Eur. J. Biochem.* **1995**, *234*, 178−183. (b) Zawia, N.; Crumpton, T.; Brydie, M.; Reddy, G.; Razmiafshari, M. *Neurotoxicology* **2000**, *21*, 1069−1080.

(6) Simons, T. *Neurotoxicology* **1993**, *14*, 77−85.

(7) (a) Warren, M. J.; Cooper, J. B.; Wood, S. P.; Shoolingin-Jordan, P. M. *Trends Biochem. Sci.* **1998**, *23*, 217−221. (b) Erskine, P. T.; Norton, E.; Cooper, J. B.; Lambert, R.; Coker, A.; Lewis, G.; Spencer, P.; Sarwar, M.; Wood, S. P.; Warren, M. J. *Biochemistry* **1999**, *38*, 4266−4276. (c) Jaffe, E. K.; Martins, J.; Li, J.; Kervinen, J.; Dunbrack, R. L. *J. Biol. Chem.* **2001**, *276*, 1531−1537.

(8) (a) Fowler, B. A. *Environ. Health Perspect.* **1998**, *106*, 1585−1587. (b) Gonick, H. C. *J. Toxicol.* **2011**, *2011*, 1−10.

(9) Stillman, M. J. *Coord. Chem. Rev.* **1995**, *144*, 461−511.

(10) Doerr, A. J.; McLendon, G. L. *Inorg. Chem.* **2004**, *43*, 7916−7925.

(11) Capdevila, M.; Bofill, R.; Palacios, O.; Atrian, S. *Coord. Chem. Rev.* **2012**, *256*, 46−62.

(12) Davidovicha, R. L.; Stavila, V.; Marinina, D. V.; Voita, E. I.; Whitmire, K. H. *Coord. Chem. Rev.* **2009**, *253*, 1316−1352.

(13) Magyar, J. S.; Weng, T.; Stern, C. M.; Dye, D. F.; Rous, B. W.; Payne, J. C.; Bridgewater, B. M.; Mijovilovich, A.; Parkin, G.; Zaleski, J. M.; Penner-Hahn, J. E.; Godwin, H. A. *J. Am. Chem. Soc.* **2005**, *127*, 9495−9505.

(14) (a) Busenlehner, L. S.; Cosper, N. J.; Scott, R. A.; Rosen, B. P.; Wong, M. D.; Giedroc, D. P. *Biochemistry* **2001**, *40*, 4426−4436. (b) Apuy, J. L.; Busenlehner, L. S.; Russell, D. H.; Giedroc, D. P. *Biochemistry* **2004**, *43*, 3824−3834. (c) Neupane, K. P.; Pecoraro, V. L. *Angew. Chem., Int. Ed.* **2010**, *49*, 8177−8180.

(15) Kirberger, M.; Yang, J. J. *J. Inorg. Biochem.* **2008**, *102*, 1901−1909.

(16) (a) He, W. G.; Chu, D. Y.; Yang, J. Y.; Yao, D. F.; Shao, M. C. *Chem. Res. Chinese U.* **1999**, *20*, 248−250. (b) Chu, D. Y.; Tang, Y.; Huan, Y.; He, W. G.; Cao, W. *Thermochim. Acta* **2000**, *352*, 205−212.

(17) Palacios, O.; Leiva-Presa, A.; Atrian, S.; Lobinski, R. *Talanta* **2007**, *72*, 480−488.

(18) Hasnain, S. S.; Kiakun, G. P. *Experientia, Suppl.* **1987**, *52*, 227−236.

(19) Senn, H. M.; Thiel, W. *Angew. Chem., Int. Ed.* **2009**, *48*, 1198−1229.

(20) (a) Warshel, A.; Levitt, M. *J. Mol. Biol.* **1976**, *103*, 227−249. (b) Singh, U. C.; Kollman, P. A. *J. Comput. Chem.* **1986**, *7*, 718−730. (c) Field, M. J.; Bash, P. A.; Karplus, M. *J. Comput. Chem.* **1990**, *11*, 700−733. (d) Maseras, F.; Morokuma, K. *J. Comput. Chem.* **1995**, *16*, 1170−1179.

(21) (a) Field, M. J. *J. Comput. Chem.* **2002**, *23*, 48−58. (b) Vreven, T.; Byun, K. S.; Komáromi, I.; Dapprich, S.; Montgomery, J. A., Jr; Morokuma, K.; Frisch, M. J. *J. Chem. Theory. Comput.* **2006**, *2*, 815−826. (c) Lin, H.; Truhlar, D. G. *Theor. Chem. Acc.* **2007**, *117*, 185−199. (d) Senn, H. M.; Thiel, W. *Curr. Opin. Chem. Biol.* **2007**, *11*, 182−187.

(22) Kägi, J. H. R.; Vallee, B. L. *J. Biol. Chem.* **1961**, *236*, 2435−2442.

(23) Sadler, P. J.; Li, H. Y.; Sun, H. Z. *Coord. Chem. Rev.* **1999**, *185−186*, 689−709.

(24) Frisch, M. J.; Trucks, G. W.; Schlegel, H. B.; Scuseria, G. E.; Robb, M. A.; Cheeseman, J. R.; Montgomery, J. J. A.; Vreven, T.; Kudin, K. N.; Burant, J. C.; Millam, J. M.; Iyengar, S. S.; Tomasi, J. V.; Barone, B.; Mennucci, M. C., Scalmani, G.; Rega, N.; Petersson, G.A.; Nakatsuji, H.; Hada, M.; Ehara, M.; Toyota, K.; Fukuda, R.; Hasegawa, J.; Ishida, M.; Nakajima, T.; Honda, Y.; Kitao, O.; Nakai, H.; Klene, M.; Li, X.; Knox, J.E.; Hratchian, H.P.; Cross, J.B.; Bakken, V.; Adamo, C.; Jaramillo, J.; Gomperts, R.; Stratmann, R.E.; Yazyev, O.; Austin, A.J.; Cammi, R.; Pomelli, C.; Ochterski, J.W.; Ayala, P.Y.; Morokuma, K.; Voth, G.A.; Salvador, P.; Dannenberg, J.J.; Zakrzewski, V.G.; Dapprich, S.; Daniels, A.D.; Strain, M.C.; Farkas, O.; Malick, D.K.; Rabuck, A.D.; Raghavachari, K.; Foresman, J.B.; Ortiz, J.V.; Cui, Q.; Baboul, A.G.; Clifford, S.; Cioslowski, J.; Stefanov, B.B.; Liu, G.; Liashenko, A.; Piskorz, P.; Komaromi, I.; Martin, R.L.; Fox, D.J.; Keith, T.; M. A. Al-Laham, Peng, C.Y.; Nanayakkara, A.; Challacombe, M.; Gill, P.M.W.; Johnson, B.; Chen, W.; Wong, M.W.; Gonzalez, C.; Pople, J.A. *Gaussian 03,* Revision E.01; Gaussian, Inc.: Wallingford, CT, 2004.

(25) (a) Li, H.; Robertson, A. D.; Jensen, J. H. *Proteins* **2005**, *61*, 704−721. (b) Bas, D. C.; Rogers, D. M.; Jensen, J. H. *Proteins* **2008**, *73*, 765−783.

(26) Peterson, K. A. *J. Chem. Phys.* **2003**, *119*, 11009−11112.

(27) (a) Casewit, C.; Colwell, K.; Rappe, A. *J. Am. Chem. Soc.* **1992**, *114*, 10035−10046. (b) Casewit, C.; Colwell, K.; Rappé, A. *J. Am. Chem. Soc.* **1992**, *114*, 10046−10053. (c) Rappé, A. K.; Casewit, C. J.; Colwell, K.; Goddard Iii, W.; Skiff, W. *J. Am. Chem. Soc.* **1992**, *114*, 10024−10035. (d) Rappe, A.; Colwell, K.; Casewit, C. *Inorg. Chem.* **1993**, *32*, 3438−3450.

(28) Bakowies, D.; Thiel, W. *J. Phys. Chem.* **1996**, *100*, 10580−10594.

(29) Bauernschmitt, R.; Ahlrichs, R. *Chem. Phys. Lett.* **1996**, *256*, 454−464.

(30) Gorelsky, S. I.; Lever, A. B. P. *J. Organomet. Chem.* **2001**, *635*, 187−196.

(31) (a) Neupane, K. P.; Pecoraro, V. L. *J. Inorg. Biochem.* **2011**, *105*, 1030−1034. (b) Bae, W.; Mehra, R. K. *J. Inorg. Biochem.* **1997**, *68*, 201−210.

(32) (a) Stillman, M. J.; Cai, W.; Zelazowski, A. J. *J. Biol. Chem.* **1987**, *262*, 4538−4548. (b) Rupp, H.; Weser, U. *Biochim. Biophys. Acta* **1978**, *533*, 209−226.

(33) (a) Rajapandian, V.; Hakkim, V.; Subramanian, V. *J. Phys. Chem. A* **2009**, *113*, 8615−8625. (b) Rajapandian, V.; Subramanian, V. *J. Phys. Chem. A* **2011**, *115*, 2866−2876.

(34) Arseniev, A.; Schultze, P.; Wörgötter, E.; Braun, W.; Wagner, G.; Vašák, M.; Kägi, J. H.; Wüthrich, K. *J. Mol. Biol.* **1988**, *201*, 637−657.

(35) (a) Kojima, Y.; Berger, C.; Vallee, B. L.; Kägi, J. *Proc. Nat. Acad. Sci. U.S.A.* **1976**, *73*, 3413−3417. (b) Vašák, M.; Berger, C.; Kägi, J. H. *FEBS Lett.* **1984**, *168*, 174−178.

(36) Bondi, A. *J. Phys. Chem.* **1964**, *68*, 441−451.

(37) Rigby, K. E.; Chan, J.; Mackie, J.; Stillman, M. J. *Proteins* **2006**, *62*, 159−172.

(38) (a) Becke, A. D. *Phys. Rev. A: At., Mol., Opt. Phys.* **1988**, *38*, 3098−3100. (b) Lee, C.; Yang, W.; Parr, R. G. *Phys. Rev. B* **1988**, *37*, 785−789. (c) Miehlich, B.; Savin, A.; Stoll, H.; Preuss, H. *Chem. Phys. Lett.* **1989**, *157*, 200−206.

(39) Perdew, J. P. *Phys. Rev. B: Condens. Matter Mater. Phys.* **1986**, *33*, 8822−8824.

(40) Wrackmeyer, B.; Horchler, K. *Annu. Rep. NMR Spectrosc.* **1990**, *22*, 249−306.

(41) Andersen, R. J.; diTargiani, R. C.; Hancock, R. D.; Stern, C. L.; Goldberg, D. P.; Godwin, H. A. *Inorg. Chem.* **2006**, *45*, 6574−6576.

(42) (a) Godwin, H. A. *Curr. Opin. Chem. Biol.* **2001**, *5*, 223−227. (b) Rous, B. W. Spectroscopic Analysis of the Interaction of Lead with the Glucocorticoid Receptor DNA-Binding Domain: A Possible Mechanism of Lead Toxicity. Northwestern University: Evanston, IL, 2004.

(43) Ercal, N.; Treeratphan, P.; Hammond, T. C.; Matthews, R. H.; Grannemann, N. H.; Spitz, D. R. *Free Radical Biol. Med.* **1996**, *21*, 157−161.

(44) Brocklehurst, K.; Gul, S.; Pickersgill, R. W. Substrate Recognition. In *Amino Acids Peptides and Proteins in Organic Chemistry, Modified Amino Acids Organocatalysis and Enzymes;* Hughes, A. B., Ed.; Wiley-VCH: New York, 2009; Vol. *2*, pp 475−506.

(45) Min, K. S.; Nakatsubo, T.; Fujita, Y.; Onosaka, S.; Tanaka, K. *Toxicol. Appl. Pharmacol.* **1992**, *113*, 299−305.

(46) Brocklehurst, K.; Watts, A.; Patel, M.; Verma, C.; Thomas, E. W. Cysteine Proteinases. In *Comprehensive Biological Catalysis;* Sinnott, M. L., Ed.; Academic Press: New York, 1998; Vol. *1*, pp 381−423.

(47) Henkel, G.; Krebs, B. *Chem. Rev.* **2004**, *104*, 801−824.

(48) Koshland, D., Jr. *Proc. Nat. Acad. Sci. U.S.A.* **1958**, *44*, 98−104.